

Highly Selective and Sensitive Aggregation-Induced Emission of Fluorescein-Coated Metal Oxide Nanoparticles

Suchetha Shetty,^[a, b] Noorullah Baig,^[a, b] Muhieddine Safa,^[c] Ridha Gharbi,^[d] Santhanagopalan Sriram,^[d] Firas Rasoul,^[c] and Bassam Alameddine^{*[a, b]}

We report the synthesis, characterization, and photophysical properties of novel metal oxide nanoparticles (NPs) coated with specially designed fluorescein substituents which are capped with electron-withdrawing groups. The fluorescein-coated nanoparticles were synthesized in excellent yields, and their structures were confirmed using various advanced spectroscopic, instrumental, and surface analysis techniques, revealing the formation of the target functionalized nanoparticles (FNPs)

which show superior chemical and thermal stabilities. In addition, the photophysical properties of the FNPs were examined using UV-visible absorption and fluorescence spectroscopy. These latter techniques disclosed aggregation-induced emission (AIE) properties for most of the target FNPs, namely those which are soluble in common organic solvents at selective concentration ranges of water fractions in the solvent mixture.

Introduction

Fluorescein and its derivatives have proved to be promising fluorophores that can be employed to design highly responsive chemosensors, fluorescent markers, bio-labels, and immunological probes.^[1] Besides its commercial availability and versatile functionalization with various side groups, fluorescein reveals excellent photophysical properties, namely, a significant absorption coefficient, a prominent fluorescent quantum yield, and great photostability. Nevertheless, fluorescein is a typical aggregation-caused quenching (ACQ) fluorescence molecule and portrays this effect majorly in solid state.^[2] As a result, fluorescein powder does not fluoresce at all, which greatly impedes its application scope, and therefore, switching fluorescein from an ACQ species into an aggregation-induced emission (AIE) molecule has been recently explored as this would undoubtedly expand its application scope.^[1a]

The design of nanostructures, namely functionalized nanoparticles (FNPs) as fluorescent probes for bioimaging and sensing applications, has seen considerable growth due to the conspicuous properties of FNPs: among others, versatile synthesis, physical and chemical stabilities as well as pronounced emission features.^[3,4] Metal oxide nanoparticles (MONPs) exhibit properties different from the ones the metal oxides show in bulk due to the high surface area-to-volume ratio of the former, which increases their surface charge and reactivity.^[4a,5] The unique properties of MONPs allow for their utilization as oil reservoir tracers,^[6] sensors for toxic gases,^[3,5a] and probes for biomedical applications,^[7] like, for example, direct or indirect biosensing,^[8] drug delivery,^[9] anticancer activity,^[10] and magnetic resonance imaging.^[11] MONPs have also been employed in the removal of various heavy metals, such as chromium, nickel, cadmium, copper, mercury, arsenic, and lead.^[12] The adsorption capacity of MONPs can be easily regenerated simply by changing the pH of the solution.^[13] Due to their ease of separation, low cost, recyclability, and high adsorption capacity, metal oxide nanoparticles are considered advantageous, both economically and technologically.^[13]


During the past two decades, there has been a growing interest in the synthesis of specially designed organic materials whose poor or non-emissive properties in solution can be substantially enhanced by inducing their aggregation through the addition of a co-solvent to the medium. This physical property, known as aggregation-induced emission (AIE), has opened new prospects in the field of luminescent materials.^[2a] For instance, AIE demonstrates the usefulness of materials displaying properties which are absent at the molecular level but can be generated when they are present as aggregates, thus, leading to potential applications.^[14] Since the development of the first AIE organic compounds, many AIE-active materials have been developed, namely by synthesizing small organic molecules and polymers.^[15] Nevertheless, fluorescent nanoparticles are considered a better choice for fluorescence imaging when compared to small molecular dyes because the


[a] S. Shetty, Dr. N. Baig, Prof. Dr. B. Alameddine
Department of Mathematics and Natural Sciences
Gulf University for Science and Technology
32093 Hawally > (Kuwait)
E-mail: alameddine.b@gust.edu.kw

[b] S. Shetty, Dr. N. Baig, Prof. Dr. B. Alameddine
Functional Materials Group – CAMB
Gulf University for Science and Technology
40006 West Mishref Kuwait

[c] Dr. M. Safa, Dr. F. Rasoul
Petroleum Research Center
Kuwait Institute for Scientific Research
70051 Safat Kuwait

[d] Dr. R. Gharbi, Dr. S. Sriram
Kuwait Oil Company
60000 Ahmadi < Kuwait

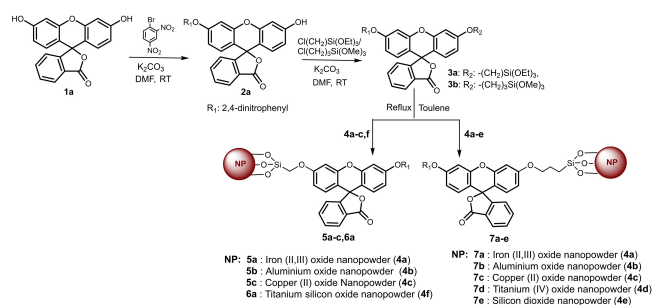
 Supporting information for this article is available on the WWW under <https://doi.org/10.1002/open.202100132>

 © 2021 The Authors. Published by Wiley-VCH GmbH. This is an open access article under the terms of the Creative Commons Attribution Non-Commercial License, which permits use, distribution and reproduction in any medium, provided the original work is properly cited and is not used for commercial purposes.

former compounds have a tunable size, superior photostability, desirable pharmacokinetic behavior, and multifunctional potential.^[16] Because of the aforementioned properties, AIE-based fluorescent nanoparticles have emerged as a novel imaging contrast agent in various biomedical areas, particularly cell imaging.^[17] We report herein the synthesis, characterization, and aggregation-induced emission (AIE) properties of several metal oxide nanoparticles (MONPs) coated with specially designed fluorescein substituents.

Results and Discussion

Scheme 1 depicts the synthesis of the target fluorescein-coated nanoparticle (FNP) derivatives. In a first step, fluorescein underwent a monosubstitution of its hydroxyl group by the electron-deficient 2,4-dinitrophenyl moiety in a typical Williamson reaction, which afforded **2a** in 80% yield. **2a** was found to be highly soluble in common organic solvents such as DCM, THF, toluene, ethyl acetate, DMF, and DMSO. Subsequently, **2a** was reacted with (chloromethyl)triethoxysilane, yielding the unsymmetrically disubstituted fluorescein derivative **3a**, which was found to be insoluble in common organic solvents, namely, DCM, THF, and toluene, but was sparingly soluble in DMF, DMSO, and ethyl acetate. To improve the solubility of the unsymmetrically disubstituted fluorescein derivative, an alter-



Scheme 1. Synthesis of NPs **5a–c**, **6a**, and **7a–e** functionalized with fluorescein derivatives.

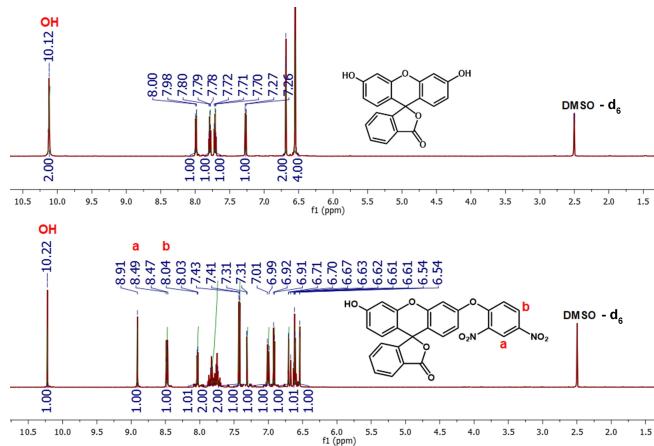


Figure 1. Comparative ¹H NMR spectra of **1a** (up) and **2a** (down) recorded in DMSO-*d*₆.

native anchoring group with a longer alkyl chain, that is, (3-chloropropyl)-trimethoxysilane was utilized. Thus, the Williamson reaction of the latter with **2a** afforded the desired compound **3b** which was found to be highly soluble in most common organic solvents. The formation of **2a** and **3a,b** was confirmed by nuclear magnetic resonance (NMR) spectroscopy, electron impact high-resolution mass spectrometry (EI-HRMS), X-ray photoelectron spectroscopy (XPS), and Fourier transform infrared spectroscopy (FTIR, see Figure 1 as well as Figures S1–S5, S7–S9, S10–S17, and S18, S19 in the Supporting Information).

Reaction of the commercially available metal oxide nanoparticles **4a–c,f** with the unsymmetrical fluorescein derivative **3a**, overnight in refluxing toluene under an inert atmosphere, afforded the desired functionalized nanoparticles (FNPs) **5a–c** and **6a** in excellent yields. The target metal oxide nanoparticles were found to be partially soluble only in ethanol but insoluble in most common organic solvents, notably DCM, THF, toluene, ethyl acetate, DMF, and DMSO. Target FNPs **7a–e** were prepared using the same procedure described above to make **5a–c** and **6a**, but using the more soluble fluorescein moiety **3b** since it contains a longer propyl spacer than the methyl one in **3a**. As expected, **7a–e** were found to have good solubility in DCM, CHCl₃, THF, DMF, DMSO, and ethanol. The formation of all the target FNPs was confirmed by FTIR, XPS, TGA, and UV-visible spectroscopy (Figure 2–5 as well as Figures S6, S10–S17, and S25–S32 in the Supporting Information).

Figure 1 depicts the compared ¹H NMR spectra of the commercially available fluorescein synthon **1a** and of the intermediate **2a** which has undergone a monosubstitution with the electron-deficient 2,4-dinitrophenyl group. The ¹H NMR spectrum of **1a** shows two characteristic hydroxyl protons at 10.12 ppm. In contrast, **2a** reveals the presence of only one –OH proton at 10.22 ppm and, in addition, the presence of two extra aromatic protons at about 8.9 and 8.4 ppm which can be attributed to the dinitrophenyl group (c.f. peaks labeled **a** and **b** in Figure 1), therefore, clearly indicating the successful formation of **2a** (see Figure S1 in the Supporting Information).

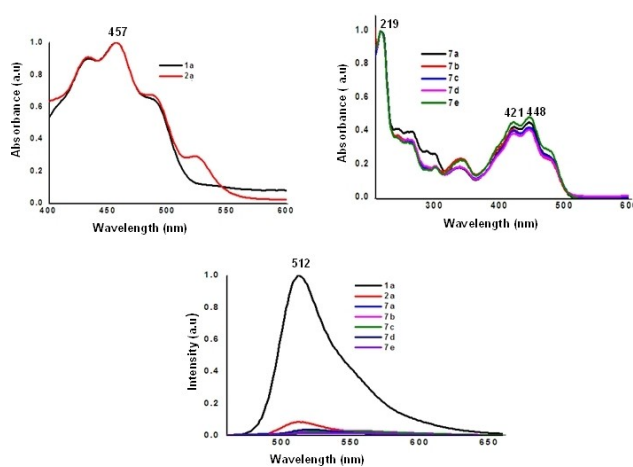


Figure 2. Normalized UV-Vis absorption ($c_M = 10^{-6}$ M in DMF and ethanol) spectra of **1a**, **2a** and **7a–e** (up) and the comparative normalized emission ($c_M = 10^{-8}$ M in DMF) spectra of **1a**, **2a** and **7a–e** (excited at 450 nm) (down).

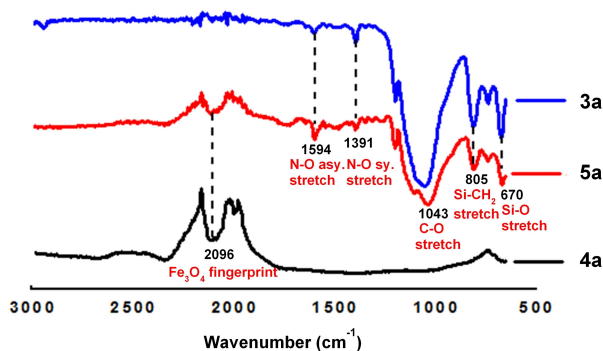


Figure 3. Comparative FTIR spectra of 4a (down), 5a (middle) and 3a (up).

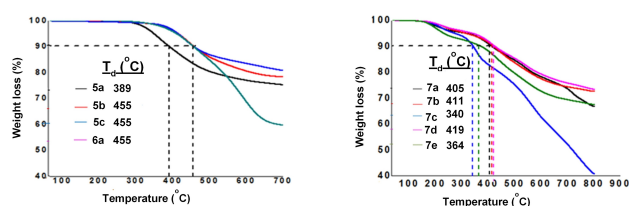


Figure 4. TGA thermograms of NPs 5a–c and 6a (left) and 7a–e (right). T_d represents the temperature of 10% weight loss.

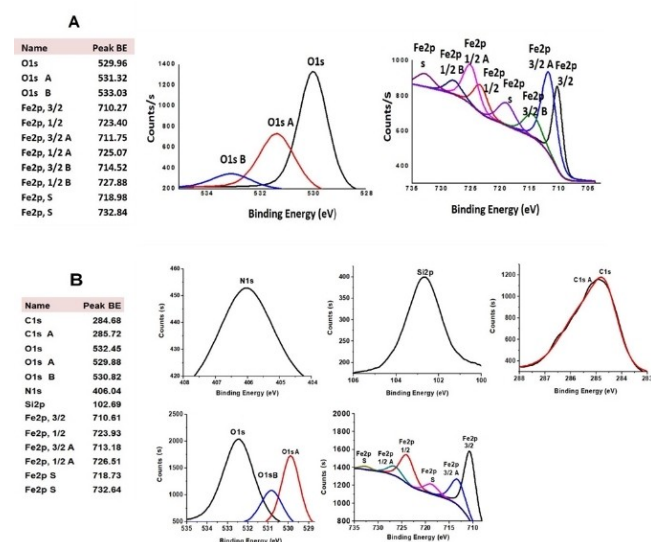


Figure 5. (A) High-resolution XPS spectra of Fe2p and O1s of 4a (B) High-resolution XPS spectra of N1s, Si2p, C1s, O1s and Fe2p of 5a.

Similarly, ^1H NMR analysis of the desired unsymmetrically disubstituted fluorescein synthon 3a, that is, the one bearing 2,4-dinitrophenyl and methyltriethoxysilane anchoring groups, reveals the absence of any hydroxyl proton peaks and portrays those that correspond to $-\text{CH}_2$ and $-\text{CH}_3$ groups in the aliphatic region, thus, confirming the formation of the desired compound (see Figure S2 in the Supporting Information). The same changes are observed in the ^1H NMR spectrum of 3b whose higher solubility than 3a allowed recording its ^{13}C NMR spectrum as well (see figures S3 and S5 in the Supporting Information).

The photophysical characteristics of synthons 1a, 2a, and target FNPs 5a–c, 6a, and 7a–e were investigated by UV-Vis absorption spectroscopy (see Figure 2 below and Figure S6 in the Supporting Information) using *N,N*-dimethylformamide (DMF) as a solvent for 1a, 2a and ethanol as a solvent for 5a–c, 6a, and 7a–e. Compounds 1a and 2a display the same features with a strong absorption band at 457 nm. The UV-Vis absorption spectra of FNPs 7a–e show absorption bands whose maximum peaks are detected at 219 nm, 421 nm, and 448 nm. Interestingly, the UV-Vis absorption spectra of 5a–c and 6a show broader absorption features with two maximum peaks at ≈ 271 nm and ≈ 512 nm (see Figure S6 in the Supporting Information). It is worthwhile to note that the emission peak of fluorescein, which is usually detected at 512 nm, is completely quenched in all the fluorescein derivatives bearing a 2,4-dinitrophenyl moiety, that is, 2a and the target FNPs 7a–e.

Comparative FTIR absorption spectra of synthons 3a, 4a, and the target FNP 5a are shown in Figure 3. Intermediate 3a shows the characteristic stretching peaks for N–O, C–O, Si–O, and Si–CH₂ at 1594 cm^{-1} , 1391 cm^{-1} , 1043 cm^{-1} , 670 cm^{-1} , and 801 cm^{-1} , respectively. It is worth mentioning that FTIR analysis of the target FNP 5a reveals the presence of all the desired stretching peaks, notably, those of the organic part (i.e. N–O, C–O, Si–O, and Si–CH₂), in addition to the fingerprint peak that is attributed to Fe₃O₄ nanoparticles at ≈ 2096 cm^{-1} . Similarly, targets 5b,c, 6a, and 7a–e display the stretching peaks which correspond to the fluorescein derivative anchor, on one hand, and those which can be attributed to the fingerprint peaks of their respective nanoparticles, on the other hand (see Figures S10–S17 in the Supporting Information).

Thermogravimetric analysis (TGA) of compounds 5a–c, 6a, and 7a–e is depicted in Figure 4, which clearly proves the superior thermal stability of the target nanoparticles revealing 10% weight loss temperatures ranging from 340 to 455 °C.

X-ray photoelectron spectroscopy (XPS) was employed to analyze the elemental composition of synthons 3a–b, 4a–f and target FNPs 5a–c, 6a, and 7a–e (Figure 5 and Figures S18–S32 in the Supporting Information). Figure 5 (B) illustrates the XPS survey-scan spectrum of 5a, thus, confirming the presence of all the constituting elements expected in the target compound, that is, carbon, nitrogen, oxygen, silicon, and iron. The binding energy for carbons C1s, C1sA at ≈ 284.68 eV and 285.72 eV are assigned to aromatic (C=C) and ether (C–O–C) groups. N1s core-level spectrum was detected at 406.04 eV, which clearly divulges the presence of nitrogen-oxygen (N–O) peaks. Peak fitting illustrates that the oxygen spectrum of 5a can be grouped into three main types O1s, O1sA, and O1sB at ≈ 532.45 eV, 529.88 eV, and 530.82 eV, respectively. The hitherto mentioned three peaks can be assigned to carbonyl (C=O), iron oxide (Fe–O), and carbonate (C–O) groups, respectively.^[18] The characteristic Si2p peak at 102.69 eV is attributed to Si–O, while the Fe2p spectrum exhibits a total of six peaks in the range of ≈ 710 –732 eV which can be assigned to Fe(II) and Fe(III) complexes.^[19] It is noteworthy that all the desired XPS peaks were detected^[19–20] for 5b,c, 6a, and 7a–e, which undoubtedly confirms the structures of the target NPs (see Figures S25–S32 in the Supporting Information).

AIE properties of Functionalized NPs

Interestingly, solid samples of the fluorescein-coated nanoparticles **7a–e** were found to be fluorescent when placed under UV light ($\lambda_{\text{ex}} = 365$ nm), contrarily to fluorescein powder **1a** which is known to suffer from typical aggregation-caused quenching (ACQ), and therefore is not fluorescent when exposed to UV light (c.f. Figure 6(A) below). This observation prompted us to investigate the emission properties of the deactivated fluorescein synthon **2a** and its unsymmetrical derivative **3b**, as well as two highly soluble FNPs, namely, **7b,d** in different solvents with various polarity. Interestingly, all the aforementioned compounds revealed similar emission spectra with fluorescence peaks that range from 514 nm to 561 nm (see Figures S34–S37 in the Supporting Information).

Subsequently, the emission intensity of FNPs **7a–e** was recorded in different THF-H₂O solvent mixtures ranging from 100% to 0% (i.e. increasing water fraction f_w , Figure 6). In a typical experiment, the emission spectra of FNP **7e** were recorded in various THF-H₂O solvent mixtures where **7e** in pure THF exhibits a very weak emission spectrum whose peak maximum corresponds to that specific for fluorescein (530 nm). Fluorescence of **7e** becomes more pronounced with an increasing water fraction until it attains a maximum emission in a 50:50 THF-H₂O mixture before it starts decreasing as f_w increases and finally shows a very weak emission peak in pure water. This behavior clearly corresponds to an aggregation-induced emission (AIE), where the addition of water to the solutions of FNPs in THF induces aggregation of the nanoparticles whose surfaces are modified with electron-deficient fluorescein derivatives (i.e. Donor-Acceptor units), which, in turn, assemble in an anti-parallel configuration with their homologues anchored to other NPs, thus intensifying the emission intensity. This latter property starts decreasing as the

water fraction increases due to the FNPs precipitation when water surpasses a certain threshold. It is noteworthy that the other FNPs **7a–d** display similar AIE properties but at different water fraction (f_w) ranges (see Figures S41–S44 in the Supporting Information). The AIE property was further corroborated by carrying out emission tests using the D–A synthons **2a** and **3b** (see Figures S39 and S40 in the Supporting Information) which disclose a similar pattern, therefore, suggesting a twisted intermolecular charge transfer mechanism.^[2a]

Conclusion

This work discloses the synthesis of nine metal oxide nanoparticles whose surfaces were functionalized with fluorescein derivatives bearing electron-withdrawing 2,4-dinitrophenyl groups. The target fluorescein-containing nanoparticles were made from inexpensive commercially available starting materials. Thorough spectroscopic characterization and instrumental analysis of the desired FNPs confirmed their formation in high purity and excellent yields. The photophysical studies of the electron-deficient fluorescein-bearing metal oxides nanoparticles **5a–c**, **6a**, and **7a–e** corroborated the significant emission suppression of the fluorescein anchoring groups. It is worthwhile to mention that FNPs **7a–e** display interesting aggregation-induced emission (AIE) properties which were studied by fluorescence spectroscopy. This work paves the way for a versatile synthetic strategy of various FNPs whose surface modification with functional groups can be tailored for a wide variety of sensing applications.

Experimental Section

General

All the reactions were carried out under an inert atmosphere using dry argon. Fluorescein (free acid) **1a**, iron (II, III) oxide nanopowder, 50–100 nm particle size, 97% trace metals basis **4a**, aluminum oxide nanopowder, <50 nm particle size **4b**, copper (II) oxide nanopowder, <50 nm particle size **4c**, titanium (IV) oxide nanopowder, 21 nm particle size, >99.5% trace metal basis **4d**, silicon dioxide nanopowder, 5–20 nm particle size, 99.5% trace metal basis **4e** and titanium silicon oxide nanopowder, <50 nm particle size, 99.8% trace metal basis **4f**, were purchased from Sigma Aldrich. All other chemical reagents were used without further purification as purchased from Aldrich, Merck, and HiMedia unless otherwise specified. The solvents, namely, DMF, ethyl acetate, hexane, DCM, DMSO, ethanol, THF, toluene, and diethyl ether, were dried and deoxygenated by bubbling with argon gas for 30 minutes. Thin-layer chromatography (TLC) was performed on aluminum sheets coated with silica gel 60 F254 and revealed using a UV lamp. NMR (¹H: 600 MHz, ¹³C: 150 MHz) spectra were recorded on Bruker BioSpin GmbH 600 MHz spectrometer using DMSO as a solvent with the chemical shifts (δ) given in ppm and referred to tetramethylsilane (TMS). UV-Vis spectra were recorded on Shimadzu UV1800 spectrophotometer. Photoluminescence (PL) spectra were recorded on an Agilent G9800 Cary Eclipse Fluorescence spectrophotometer. X-ray Photoelectron Spectroscopy (XPS) data were recorded on a Thermo ESCALAB 250 Xi using a monochromatic Al K α -radiation source (1486.6 eV) with a spot size of 850 μm . Spectra acquisition

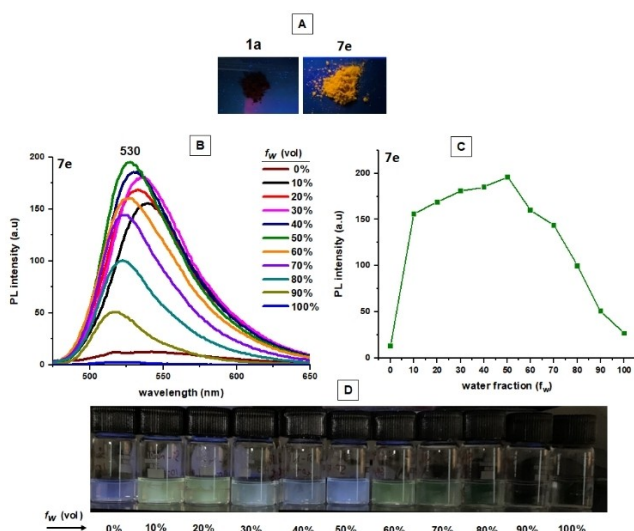


Figure 6. (A) Solid state fluorescence images of **1a** and **7e** (B) Emission spectra of **7e** in THF/water mixtures (0–100%) (C) Plot of maximum emission intensity of **7e** ($c_M = 10^{-6}$ M) versus water fraction (D) Photographs of **7e** in THF/water (0–100%) mixtures taken under UV illumination ($\lambda_{\text{ex}} = 365$ nm).

and processing were carried out using the software Thermo Advantage Version 4.87. The base pressure in the XPS analysis chamber was in the range 10^{-10} to 10^{-9} Torr. The analyzer was operated with pass energy of 20 eV, dwell time of 50 min, and with a step size of 0.1 eV. Thermogravimetric Analysis (TGA) was recorded on Shimadzu TGA-60H (Kyoto, Japan) analyzer and was used to measure the thermal stability of composites from room temperature to 800 °C with a heating rate of 10 °C min⁻¹ under an inert atmosphere using pure nitrogen. FTIR spectra were recorded on Agilent Cary 630 FTIR instrument. Electron impact high-resolution mass spectra (EI-HRMS) were recorded on a Thermo (DFS) with a standard PFK (perfluorokerosene) as lock mass. The analyzed data is converted to accurate mass with the help of X-Calibur accurate mass calculation software.

Synthesis

Synthesis of 2a

2a was synthesized following the reported procedure^[21] with: fluorescein **1a** (1 g, 3.0 mmol, 1 equiv.), 1-bromo-2,4-dinitrobenzene (0.7 g, 3.0 mmol, 1 equiv.), K₂CO₃ (0.46 g, 3.3 mmol, 1.1 eq.), and 30 mL anhydrous DMF mixed in a Schlenk tube under a positive stream of argon and the mixture was stirred at room temperature for 24 h. The reaction mixture was extracted with ethyl acetate from a 0.1 M lithium chloride solution (2 × 100 mL) and the organic phase was washed with water (3 × 100 mL). The organic layer was then concentrated and the pure compound was isolated by silica gel column chromatography using ethyl acetate/hexane (30:70 by volume) as eluent yielding a yellow solid (80%); ¹H NMR (DMSO-d₆, 600 MHz, ppm): δ 10.22 (s, 1H, OH), 8.91 (s, 1H, ArH), 8.49–8.47 (m, 1H, ArH), 8.04–8.03 (d, *J* = 7.2 Hz, 1H, ArH) 7.84–7.73 (m, 2H, ArH), 7.43 (d, *J* = 9 Hz, 2H, ArH), 7.31 (d, *J* = 2.4 Hz, 1H, ArH), 7.01–6.99 (m, 1H, ArH), 6.92 (d, *J* = 9 Hz, 1H, ArH), 6.71 (d, *J* = 2.4 Hz, 1H, ArH), 6.61 (d, *J* = 2.4 Hz, 1H, ArH) 6.54 (s, 1H, ArH); ¹³C NMR (DMSO-d₆, 150 MHz, ppm): δ 170.33, 168.52, 159.73, 159.45, 155.80, 155.61, 153.71, 152.25, 151.90, 142.25, 139.97, 130.37, 129.73, 125.79, 124.84, 121.93, 120.96 116.50, 115.68, 113.20, 109.10, 107.98, 102.23, 81.87; EI-HRMS: *m/z* calculated for (M⁺) C₂₆H₁₄N₂O₉ 498.0694, found 498.0695; UV-Vis: (DMF, 10⁻⁶ M), λ_{max} [nm] = 457.

Synthesis of 3a

2a (0.8 g, 1.6 mmol, 1 equiv.), (chloromethyl)triethoxysilane (0.34 g, 1.6 mmol, 1 equiv.), K₂CO₃ (0.24 g, 1.8 mmol, 1.1 eq.), and 30 mL anhydrous DMF were added in a Schlenk tube under a positive stream of argon and the mixture was stirred at room temperature for 24 h. The reaction mixture was then extracted with ethyl acetate from a 0.1 M lithium chloride solution (2 × 100 mL), and the organic phase was washed with water (3 × 100 mL). The organic layer was concentrated, and the pure compound was isolated by suspending in DCM followed by filtration and washed with diethyl ether. Red solid. Yield: (52%); ¹H NMR (DMSO-d₆, 600 MHz, ppm): δ 8.92 (s, 1H, ArH), 8.47 (br, 1H, ArH), 8.06–8.04 (m, 1H, ArH) 7.87–7.76 (m, 4H, ArH), 7.42–7.34 (m, 1H, ArH), 7.01–6.96 (m, 2H, ArH), 6.96–6.75 (m, 3H, ArH), 4.34 (t, *J* = 4.8 Hz, 6H, -CH₂), 3.87 (s, 2H, -CH₂), 1.05 (t, *J* = 6.6 Hz, 9H, -CH₃); FTIR [cm⁻¹]: 1390 (N–O), 1043 (C–O), 801 (Si–CH₂), 670 (Si–O).

Synthesis of 5a (Procedure A)

A Schlenk tube was charged with iron (II, III) oxide nanopowder **4a** (69 mg, 0.3 mmol 1 equiv.) and **3a** (100 mg, 0.15 mmol, 0.5 equiv.) in 20 mL anhydrous toluene, and the reaction mixture was refluxed

for 12 h under argon. The product was isolated by filtration and washed several times with anhydrous toluene, DCM, THF, and ethanol. Off-white solid (yield: 89%). UV-Vis: (Ethanol, 10⁻⁶ M), λ_{max} [nm] = 271 and 512; FTIR [cm⁻¹]: 2094 (Fe₃O₄ fingerprint), 1390 (N–O), 1043 (C–O), 801 (Si–CH₂), 670 (Si–O).

Synthesis of 5b

5b was prepared following the procedure A with aluminum oxide nano powder **4b** (30 mg, 0.3 mmol, 1 equiv.) and **3a** (100 mg, 0.15 mmol, 0.5 equiv.) in 20 mL anhydrous toluene. Yellow solid (yield: 83%). UV-Vis: (Ethanol, 10⁻⁶ M), λ_{max} [nm] = 271 and 512, FTIR [cm⁻¹]: 3410 (Al₂O₃ fingerprint), 1394 (N–O), 1051 (C–O), 801 (Si–CH₂), 670 (Si–O).

Synthesis of 5c

5c was prepared following procedure A with copper (II) oxide nano powder **4c** (24 mg, 0.3 mmol, 1 equiv.) and **3a** (100 mg, 0.15 mmol, 0.5 equiv.) in 20 mL of anhydrous toluene. Grey solid (yield: 81%). UV-Vis: (Ethanol, 10⁻⁶ M), λ_{max} [nm] = 271 and 512, FTIR [cm⁻¹]: 2094 (CuO fingerprint), 1390 (N–O), 1043 (C–O), 801 (Si–CH₂), 670 (Si–O).

Synthesis of 6a

6a was prepared following procedure A with titanium silicon oxide nano powder **4f** (40 mg, 0.3 mmol, 1 equiv.) and **3a** (100 mg, 0.15 mmol, 0.5 equiv.) in 20 mL of anhydrous toluene. Yellow solid (yield: 88%). UV-Vis: (Ethanol, 10⁻⁶ M), λ_{max} [nm] = 271 and 512, FTIR [cm⁻¹]: 3496 (TiO₂-SiO₂ fingerprint), 1394 (N–O), 1051 (C–O), 801 (Si–CH₂), 659 (Si–O).

Synthesis of 3b

2a (6 g, 12 mmol, 1 equiv.), (3-chloropropyl)trimethoxysilane (2 g, 12 mmol, 1 equiv.), K₂CO₃ (1.8 g, 13.2 mmol, 1.1 equiv.), and 180 mL of anhydrous DMF were mixed in a Schlenk tube under a positive stream of argon and the mixture was stirred at room temperature for 24 h. The reaction mixture was extracted with ethyl acetate from a 0.1 M lithium chloride solution (2 × 100 mL) and the organic phase was washed with water (3 × 100 mL). The organic layer was completely dried and the residue was suspended in water and sonicated before filtration under reduced pressure. The precipitate was washed exhaustively with petroleum ether yielding a red solid (95%); ¹H NMR (CD₂Cl₂, 600 MHz, ppm): δ 8.72 (s, 1H, ArH), 8.46 (br, 1H, ArH), 8.28–8.24 (m, 1H, ArH) 7.75–7.68 (m, 4H, ArH), 7.32 (br, 1H, ArH), 7.24 (m, 1H, ArH), 6.96 (br, 1H, ArH), 6.86–6.76 (m, 3H, ArH), 4.08 (s, 2H, -CH₂), 3.55 (br, 9H, -CH₃), 1.86 (br, 2H, -CH₂), 0.78 (br, 2H, -CH₂); ¹³C NMR (CD₂Cl₂, 150 MHz, ppm): δ 185.56, 165.95, 163.84, 159.27, 157.80, 156.13, 154.60, 134.97, 133.08, 131.42, 130.98, 130.74, 130.02, 129.88, 129.60, 129.37, 122.15, 117.90, 115.27, 114.30, 105.83, 105.65, 101.11, 70.00, 57.99, 47.72, 14.48, 10.29; FTIR [cm⁻¹]: 1394 (N–O), 1051 (C–O), 801 (Si–CH₂), 670 (Si–O).

Synthesis of 7a (Procedure B)

A Schlenk tube was charged with iron (II, III) oxide nano powder **4a** (700 mg, 3.0 mmol, 1 equiv.) and **3b** (1 g, 1.5 mmol, 0.5 equiv.) in 200 mL of anhydrous toluene. The reaction mixture was refluxed for 12 h under argon. The product was isolated by filtration using Millipore, and the precipitate was washed several times with anhydrous toluene followed by ethanol. Grey solid (yield: 92%). UV-Vis: (Ethanol, 10⁻⁶ M), λ_{max} [nm] = 219, 421 and 448; FTIR [cm⁻¹]:

2105 (Fe₃O₄ fingerprint), 1587 (C–C), 1375 (N–O), 1248 (C–N), 1099 (C–O), 846 (Si–CH₂), 659 (Si–O).

Synthesis of 7b

7b was prepared following procedure B with aluminum oxide nano powder **4b** (300 mg, 3.0 mmol, 1 equiv.) and **3b** (1 g, 1.5 mmol, 0.5 equiv.) in 200 mL of anhydrous toluene. Yellow solid (yield: 88%). UV-Vis: (Ethanol, 10⁻⁶ M), λ_{max} [nm]=219, 421 and 448; FTIR [cm⁻¹]: 3373 (Al₂O₃ fingerprint), 1587 (C–C), 1375 (N–O), 1244 (C–N), 1077 (C–O), 753 (Si–CH₂), 663 (Si–O).

Synthesis of 7c

7c was prepared following procedure B with copper (II) oxide nano powder **4c** (240 mg, 3.0 mmol, 1 equiv.) and **3b** (1 g, 1.5 mmol, 0.5 equiv.) in 200 mL of anhydrous toluene. Grey solid (yield: 82%). UV-Vis: (Ethanol, 10⁻⁶ M), λ_{max} [nm]=219, 421 and 448; FTIR [cm⁻¹]: 2098 (CuO fingerprint), 1587 (C–C), 1375 (N–O), 1248 (C–N), 1099 (C–O), 846 (Si–CH₂), 659 (Si–O).

Synthesis of 7d

7d was prepared following procedure B with titanium (IV) oxide nano powder **4d** (240 mg, 3.0 mmol, 1 equiv.) and **3b** (1 g, 1.5 mmol, 0.5 equiv.) in 200 mL of anhydrous toluene. Yellow solid (yield: 87%). UV-Vis: (Ethanol, 10⁻⁶ M), λ_{max} [nm]=219, 421 and 448; FTIR [cm⁻¹]: 3358 (TiO₂ fingerprint), 1587 (C–C), 1375 (N–O), 1244 (C–N), 1077 (C–O), 752 (Si–CH₂) and 663 (Si–O).

Synthesis of 7e

7e was prepared following procedure B with silicon oxide nano powder **4e** (182 mg, 3.0 mmol, 1 equiv.) and **3b** (1 g, 1.5 mmol, 0.5 equiv.) in 200 mL of anhydrous toluene. Yellow solid (yield: 84%). UV-Vis: (Ethanol, 10⁻⁶ M), λ_{max} [nm]=279, 421 and 448; FTIR [cm⁻¹]: 1587 (C–C), 1375 (N–O), 1244 (C–N), 1077 (C–O), 752 (Si–CH₂), 663 (Si–O).

Acknowledgements

The authors would like to acknowledge the financial support of Kuwait Oil Company (KOC) and Kuwait Institute for Scientific Research (KISR) for funding of this study. All participating members of this project are gratefully thanked for their support of this work. B. A. would like to thank the Kuwait Foundation for the Advancement of Sciences (KFAS, PN17-34SC-01). Many thanks are extended to the staff at the Functional Materials Group at GUST and Petroleum Research Center (PRC) at KISR for their full support.

Conflict of Interest

The authors declare no conflict of interest.

Keywords: aggregation-induced emission · fluorescence · nanomaterials · nanoparticles synthesis · X-ray photoelectron spectroscopy

- a) S. Feng, S. Gong, G. Feng, *Chem. Commun.* **2020**, 56, 2511–2513; b) H. Zheng, X.-Q. Zhan, Q.-N. Bian, X.-J. Zhang, *Chem. Commun.* **2013**, 49, 429–447.
- a) J. Mei, Y. Hong, J. W. Y. Lam, A. Qin, Y. Tang, B. Z. Tang, *Adv. Mater.* **2014**, 26, 5429–5479; b) R. T. K. Kwok, C. W. T. Leung, J. W. Y. Lam, B. Z. Tang, *Chem. Soc. Rev.* **2015**, 44, 4228–4238.
- Z. Li, S. Yan, S. Zhang, J. Wang, W. Shen, Z. Wang, Y. Q. Fu, *J. Alloys Compd.* **2019**, 770, 721–731.
- a) Z. Yuan, F. Lu, M. Peng, C.-W. Wang, Y.-T. Tseng, Y. Du, N. Cai, C.-W. Lien, H.-T. Chang, Y. He, E. S. Yeung, *Anal. Chem.* **2015**, 87, 7267–7273; b) M. Chen, M. Yin, *Prog. Polym. Sci.* **2014**, 39, 365–395; c) J. Liu, X. Yang, X. He, K. Wang, Q. Wang, Q. Guo, H. Shi, J. Huang, X. Huo, *Sci. China Chem.* **2011**, 54, 1157; d) D. Jańczewski, Y. Zhang, G. K. Das, D. K. Yi, P. Padmanabhan, K. K. Bhakoo, T. T. Y. Tan, S. T. Selvan, *Microsc. Res. Tech.* **2011**, 74, 563–576; e) M. Hahn, A. Singh, P. Sharma, S. Brown, B. Moudgil, *Anal. Bioanal. Chem.* **2010**, 399, 3–27; f) M. De, P. S. Ghosh, V. M. Rotello, *Adv. Mater.* **2008**, 20, 4225–4241.
- a) J. Lawrence, R. v Hal, J. Lam, (Schlumberger Technology Corporation United States of America), USOO9052289B2, **2015**; b) Z.-L. Song, Z. Chen, X. Bian, L.-Y. Zhou, D. Ding, H. Liang, Y.-X. Zou, S.-S. Wang, L. Chen, C. Yang, X.-B. Zhang, W. Tan, *J. Am. Chem. Soc.* **2014**, 136, 13558–13561; c) X. Tian, Z. Dong, R. Wang, J. Ma, *Sens. Actuators B* **2013**, 183, 446–453.
- a) S. Chang, S. L. Eichmann, T.-Y. S. Huang, W. Yun, W. Wang, *J. Phys. Chem. C* **2017**, 121, 8070–8076; b) J. R. Cox, M. Alsenani, S. E. Miller, J. A. Roush, R. Shi, H. Ow, S. Chang, A. A. Kmetz, S. L. Eichmann, M. E. Poitzsch, *ACS Appl. Mater. Interfaces* **2017**, 9, 13111–13120.
- a) R. Serrano García, S. Stafford, Y. K. Gun'ko, *Appl. Sci.* **2018**, 8; b) K. Cherukula, K. M. Lekshmi, S. Uthaman, K. Cho, C.-s. Cho, I. Park, *Nanomaterials* **2016**, 6, 76–102; c) P. Padmanabhan, A. Kumar, S. Kumar, R. K. Chaudhary, B. Gulyás, *Acta Biomater.* **2016**, 41, 1–16; d) Q. Le Trequesser, H. Seznec, M.-H. Delville, *Nanotechnol. Rev.* **2013**, 2, 125–169; e) K. Yan, P. Li, H. Zhu, Y. Zhou, J. Ding, J. Shen, Z. Li, Z. Xu, P. K. Chu, *RSC Adv.* **2013**, 3, 10598–10618; f) S.-H. Huang, R.-S. Juang, *J. Nanopart. Res.* **2011**, 13, 4411; g) M. Mahmoudi, V. Serpooshan, S. Laurent, *Nanoscale* **2011**, 3, 3007–3026; h) T. D. Schladt, K. Schneider, H. Schild, W. Tremel, *Dalton Trans.* **2011**, 40, 6315–6343; i) J. Gao, H. Gu, B. Xu, *Acc. Chem. Res.* **2009**, 42, 1097–1107; j) I. Hilger, R. Hergt, W. Kaiser, *IEE Proc. Nanobiotechnol.* **2005**, 152 1, 33–39.
- D. Alcantara, S. Lopez, M. L. García-Martin, D. Pozo, *Nanomedicine* **2016**, 12, 1253–1262.
- K. Hola, Z. Markova, G. Zoppellaro, J. Tucek, R. Zboril, *Biotechnol. Adv.* **2015**, 33, 1162–1176.
- a) M. J. Akhtar, M. Ahamed, S. Kumar, M. M. Khan, J. Ahmad, S. A. Alrokayan, *Int. J. Nanomed.* **2012**, 7, 845–857; b) A. Espinosa, R. Di Corato, J. Kolosnjaj-Tabi, P. Flaud, T. Pellegrino, C. Wilhelm, *ACS Nano* **2016**, 10, 2436–2446.
- a) T.-H. Shin, Y. Choi, S. Kim, J. Cheon, *Chem. Soc. Rev.* **2015**, 44, 4501–4516; b) R. Augustine, A. P. Mathew, A. Sosnik, *Appl. Mater. Res.* **2017**, 7, 91–103.
- P. Sanga, Y. Iradukunda, J. C. Munyemana, *Journal of Geoscience and Environment Protection* **2018**, 06, 216–226.
- S. Singh, V. Kumar, R. Romero, K. Sharma, J. Singh, in: *Nanobiotechnology in Bioformulations* (Eds.: R. Prasad, V. Kumar, M. Kumar, D. Choudhary), Springer International Publishing, Cham, **2019**, pp. 395–418.
- a) B. Tang, Z. Zhao, H. Zhang, W. Jacky, *Angew. Chem. Int. Ed.* **2020**, 59; b) C. Xiaolei, B. Liu, *Angew. Chem. Int. Ed.* **2020**, 59; c) V. M. Granchak, T. V. Sakhno, I. V. Korotkova, Y. E. Sakhno, S. Y. Kuchmy, *Theor. Exp. Chem.* **2018**, 54, 147–177; d) H. Gao, X. Zhao, S. Chen, *Molecules* **2018**, 23; e) N. Alifu, X. Dong, D. Li, X. Sun, A. Zebibula, D. Zhang, G. Zhang, J. Qian, *Mater. Chem. Front.* **2017**, 1, 1746–1753.
- a) P. Alam, C. Climent, P. Alemany, I. R. Laskar, *J. Photochem. Photobiol. C* **2019**, 41, 100317; b) W. Huang, M. Bender, K. Seehafer, I. Wacker, R. R. Schröder, U. H. F. Bunz, *Macromolecules* **2018**, 51, 1345–1350; c) M. Desroches, J.-F. Morin, *Org. Lett.* **2018**, 20, 2797–2801; d) Z. Wang, C. Wang, Y. Fang, H. Yuan, Y. Quan, Y. Cheng, *Polym. Chem.* **2018**, 9, 3205–3214; e) A. C. B. Rodrigues, J. Pina, W. Dong, M. Forster, U. Scherf, J. S. Seixas de Melo, *Macromolecules* **2018**, 51, 8501–8512; f) L. Zong, Y. Xie, C. Wang, J.-R. Li, Q. Li, Z. Li, *Chem. Commun.* **2016**, 52, 11496–11499; g) J. Yang, J. Huang, Q. Li, Z. Li, in *Aggregation-Induced Emission: Materials and Applications Volume 1*, Vol. 1226, American Chemical Society, **2016**, pp. 61–83; h) Z. Zhao, B. He, B. Z. Tang, *Chem. Sci.* **2015**, 6, 5347–5365; i) W. Z. Yuan, Y. Gong, S. Chen, X. Y. Shen, J. W. Y. Lam, P. Lu, Y. Lu, Z. Wang, R. Hu, N. Xie, H. S. Kwok, Y. Zhang, J. Z. Sun, B. Z. Tang, *Chem. Mater.* **2012**, 24, 1518–1528; j) K. K.-W. Lo, A. W.-T. Choi,

- W. H.-T. Law, *Dalton Trans.* **2012**, 41, 6021–6047; k) F. Würthner, T. E. Kaiser, C. R. Saha-Möller, *Angew. Chem. Int. Ed.* **2011**, 50, 3376–3410; *Angew. Chem.* **2011**, 123, 3436–3473.
- [16] a) B. Yang, X. Zhang, X. Zhang, Z. Huang, Y. Wei, L. Tao, *Mater. Today* **2016**, 19, 284–291; b) X. Wu, X. He, K. Wang, C. Xie, B. Zhou, Z. Qing, *Nanoscale* **2010**, 2, 2244–2249; c) Y.-P. Ho, K. W. Leong, *Nanoscale* **2010**, 2, 60–68; d) S. Chandra, P. Das, S. Bag, D. Laha, P. Pramanik, *Nanoscale* **2011**, 3, 1533–1540; e) A. Shiohara, S. Prabakar, A. Faramus, C.-Y. Hsu, P.-S. Lai, P. T. Northcote, R. D. Tilley, *Nanoscale* **2011**, 3, 3364–3370.
- [17] a) X. Zhang, K. Wang, M. Liu, X. Zhang, L. Tao, Y. Chen, Y. Wei, *Nanoscale* **2015**, 7, 11486–11508; b) D. Ding, J. Liang, H. Shi, R. T. K. Kwok, M. Gao, G. Feng, Y. Yuan, B. Z. Tang, B. Liu, *J. Mater. Chem. B* **2014**, 2, 231–238; c) W. Qin, D. Ding, J. Liu, W. Z. Yuan, Y. Hu, B. Liu, B. Z. Tang, *Adv. Funct. Mater.* **2012**, 22, 771–779; d) Y. Yuan, R. T. K. Kwok, B. Z. Tang, B. Liu, *J. Am. Chem. Soc.* **2014**, 136, 2546–2554; e) X. Xue, Y. Zhao, L. Dai, X. Zhang, X. Hao, C. Zhang, S. Huo, J. Liu, C. Liu, A. Kumar, W.-Q. Chen, G. Zou, X.-J. Liang, *Adv. Mater.* **2014**, 26, 712–717.
- [18] a) S. Shetty, N. Baig, S. Al-Mousawi, F. Al-Sagheer, B. Alameddine, *Polymer* **2019**, 178, 121606; b) P. L. Cheung, S. K. Lee, C. P. Kubiak, *Chem. Mater.* **2019**, 31, 1908–1919.
- [19] C. Lin, J.-Y. Hong, C.-N. Yen, S.-Y. Tong, M.-J. Tung, H.-W. Shiu, C.-H. Chen, M.-T. Lin, *Jpn. J. Appl. Phys.* **2015**, 54, 033002.
- [20] X. Zhang, P. Gu, X. Li, G. Zhang, *Chem. Eng. J.* **2017**, 322, 129–139.
- [21] H.-Y. Liu, M. Zhao, Q.-L. Qiao, H.-J. Lang, J.-Z. Xu, Z.-C. Xu, *Chin. Chem. Lett.* **2014**, 25, 1060–1064.

Manuscript received: June 2, 2021

Revised manuscript received: October 6, 2021